UDC 621.313: 621.92: 537.8 https://doi.org/10.20998/2074-272X.2021.4.02

V.I. Milykh, M.G. Tymin

A COMPARATIVE ANALYSIS OF THE PARAMETERS OF A ROTATING MAGNETIC FIELD INDUCTOR WHEN USING CONCENTRIC AND LOOP WINDINGS

Introduction. *Three-phase inductors of a rotating magnetic field are used in grinders, separators and stirrers for the technological processing of bulk and liquid substances. This occurs in a cylindrical working chamber under the influence of ferromagnetic elements in the form of pieces of iron wire, which move together with the field.* ***Problem.*** *By analogy with three-phase induction motors, for the stator of inductors a concentric winding is adopted, which is a diametric single-layer winding. When moving from such motors to an inductor, its operating conditions have changed due to the significantly increased non-magnetic space inside the inductor compared to the motor clearances. The difference in the frontal parts of the phase windings has become essential for the electromagnetic parameters and the structure of the magnetic field in the inductor working chamber. Therefore, a loop shortened stator winding, which is symmetrical, can be considered as an alternative to a concentric diametric winding.* ***Goal.*** *The aim of the work is to compare the dimensional and electromagnetic parameters of a rotating magnetic field inductor in two versions of its three-phase winding: concentric single-layer diametrical and loop shortened two-layer.* ***Methodology.*** *Comparison of the windings is carried out through a detailed analysis of the geometrical parameters of their frontal parts, as well as through numerical-field calculations of the electromagnetic parameters of the inductor as a whole and the distribution of the magnetic field in its working chamber.* ***Results.*** *A significant difference in the geometrical parameters of the frontal parts of the two windings under inductor conditions was revealed. The loop version of the winding makes it possible to reduce the length of the winding conductor, its active resistance, as well as the reactance of its frontal dissipation. At the same time the asymmetry of the phase windings is excluded and an increase in the homogeneity of the magnetic field in the inductor working chamber is provided.* ***Originality.*** *The scientific novelty of the work lies in the development of a method of comparative analysis of the windings under the conditions of the rotating magnetic field inductor and in revealing the advantages of a loop shortened winding compared to the used concentric diametric winding.* ***Practical value.*** *The loop shortened stator winding recommended for the inductor will eliminate the asymmetry of its electromagnetic system. Thereby, the quality of its work in the technological processing of different substances is significantly increased due to ensuring the homogeneity of the magnetic field in the working chamber. At the same time, the copper conductor of the winding is still saved, and the efficiency of the inductor is also increased by reducing the power of electrical losses.* References 12, tables 5, figures 12.

Key words: **rotating magnetic field inductor, stator winding versions, geometrical and electromagnetic parameters.**

Розглянутий трифазний індуктор обертового магнітного поля для технологічної обробки різних речовин. Виконаний аналіз переваг і недоліків петльової укороченої обмотки його статора, яка пропонується як альтернатива використовуваної концентричної діаметральної обмотки. Порівняння обмоток проводиться за допомогою детального аналізу геометричних параметром їх лобових частин, а також електромагнітних параметрів індуктора в цілому за допомогою чисельно-польових розрахунків. Виявлено, що петльовий варіант дозволяє зменшити активний і реактивний опори лобового розсіяння обмотки і, що найсуттєвіше, виключити несиметрію фазних обмоток, забезпечуючи підвищення однорідності магнітного поля в робочій камері індуктора. Бібл. 12, табл. 5, рис. 12.

Ключові слова: **індуктор обертового магнітного поля, варіанти обмотки статора, геометричні і електромагнітні параметри.**

Рассмотрен трехфазный индуктор вращающегося магнитного поля для технологической обработки разных веществ. Выполнен анализ преимуществ и недостатков петлевой укороченной обмотки его статора, которая предлагается как альтернатива используемой концентрической диаметральной обмотки. Сравнение обмоток проводится посредством детального анализа геометрических параметром их лобовых частей, а также электромагнитных параметров индуктора в целом посредством численно-полевых расчетов. Выявлено, что петлевой вариант позволяет уменьшить активное и реактивное сопротивления лобового рассеяния обмотки и, что наиболее существенно, исключить несимметрию фазных обмоток, обеспечивая повышение однородности магнитного поля в рабочей камере индуктора. Библ. 12, табл. 5, рис. 12.

Ключевые слова: **индуктор вращающегося магнитного поля, варианты обмотки статора, геометрические и электромагнитные параметры.**

Introduction. Technological processing of various materials in grinders, separators and mixers is carried out using a magnetic field [1-8]. Including bulk and liquid substances are processed in inductors of a rotating magnetic field (IRMF) – electromagnetic mills [3, 4, 6-8]. This occurs under the influence of ferromagnetic elements (FEs) in the form of pieces of iron wire in a cylindrical working chamber, through which in the axial direction the processed substance is passed. Such elements move with a magnetic field, creating a so-called «vortex layer» in the chamber.

Initially, the inductors had a ferromagnetic core with three explicit poles, which housed the coils of a three-phase AC system [1]. This inductor design was replaced by an implicit-pole electromagnetic system similar to the stator of three-phase induction motors (TIM).

The energy level and dimensions of the inductors which are developed and operated correspond to the TIM with power of the order of units and tens of kilowatts. Therefore, taking into account the experience of their creation and operation [9], for inductors a fairly simple three-phase concentric diametric single-layer winding is adopted.

However, during the transition from TIM to the inductor, the conditions of its operation have changed

significantly due to the fact that the non-magnetic space inside the inductor has increased by two orders of magnitude compared to the gaps of the motor. If earlier the voltage drop across the active resistance and reactive resistance of the frontal scattering of the phase windings were units of percent of the electromotive force (EMF) on the active length of the machine, then in the inductor they are already commensurate. Under such conditions, the asymmetry of the frontal parts of the phase windings, which is inherent in the specified concentric winding, becomes significant. Also unfavorable is the pronounced «stepwise» distribution of the magnetomotive force (MMF) of the three-phase diametrical winding along the line of the boring circle of the stator core.

The theory of electric machines shows that a three-phase loop shortened winding, which is two-layer is deprived of these shortcomings [9]. However, for technological reasons, such a winding is considered acceptable in TIMs only as their power and dimensions increase.

The feasibility of using a loop winding in the IRMF instead of concentric one can be identified by comparing them in its conditions. The adequacy of this comparison has recently increased due to the development of methods for calculating electromagnetic parameters and characteristics of the inductor based on numerical calculations of magnetic fields [10, 11].

The goal of this work is to compare the dimensional and electromagnetic parameters of the inductor of a rotating magnetic field with two variants of its three-phase winding: concentric single-layer diametrical and loop shortened two-layer.

Object of study. The three-phase inductor is bipolar. Its electromagnetic system is given by its cross section in Fig. 1. The geometric parameters of the inductor are due to given for technological reasons the active length l_a = 250 mm and the radius of the inner surface r_{ki} = 47 mm of the working chamber at the average value of the magnetic flux density in it B_{av} = 0.12 T. This is due to the axial length of the stator core l_s, which is equal to l_a, the radii of its boring r_{si} = 0.06 m and the outer surface r_{si} = 0.109 m.

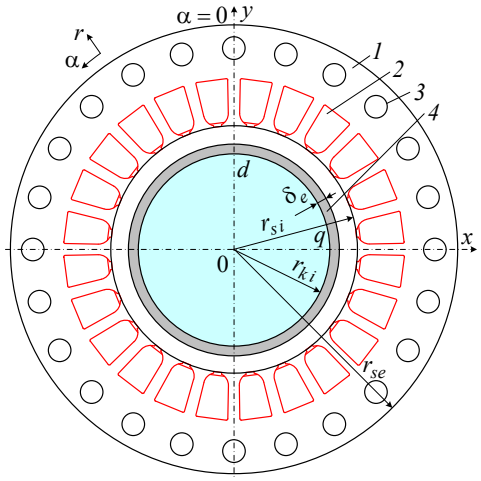

Fig. 1. Cross section of the IRMF electromagnetic system: *1* – laminated ferromagnetic core; *2* – slots with winding; *3* – ventilation ducts; *4* – shell of the working chamber

The core is made of electrical steel grade 2212 with thickness of 0.5 mm and has filling factor K_{Fe} = 0.95. The connection scheme of the winding is «star», and its phase has N_s = 72 turns. The shell of the chamber is δ_e = 5 mm thick and is made of non-magnetic stainless steel.

The inductor with the listed parameters was investigated in [11], where the calculation revealed the rated phase voltage of the stator winding U_{sN} = 100 V at frequency f_s = 50 Hz, but there another problem has been considered.

The structures of the compared variants of the winding – concentric diametric and loop shortened are given in Fig. 2, 3, where τ_p is the pole step. And for the second of them the coefficient of relative shortening β_s = 10/12 is chosen.

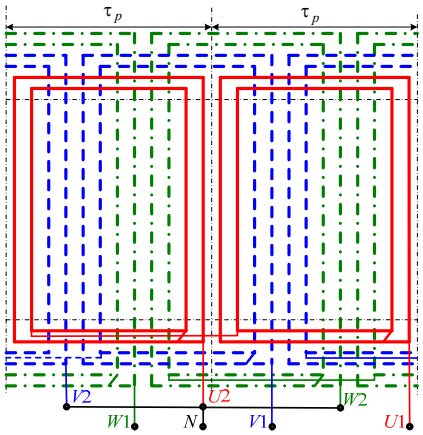

Fig. 2. Three-phase two-pole concentric single-layer stator winding

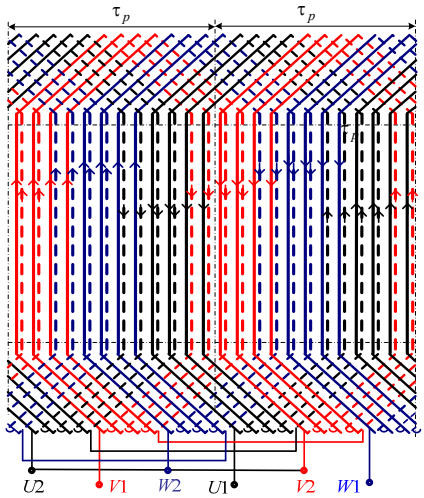

Fig. 3. Three-phase two-pole loop two-layer with shortened step stator winding

The distribution of phase windings in the slots of the stator is shown in Fig. 4, 5 in cross section of the electromagnetic system of the inductor.

In the example in Fig. 4 in the working chamber there are no FEs, and this corresponds to the ideal idle (II). In Fig. 5 the chamber is filled with FEs, which are oriented along the *y*-axis, and the magnetic field is rotated by the angle Θ, which is, as considered in [10], the load angle in the corresponding mode of operation of the inductor.

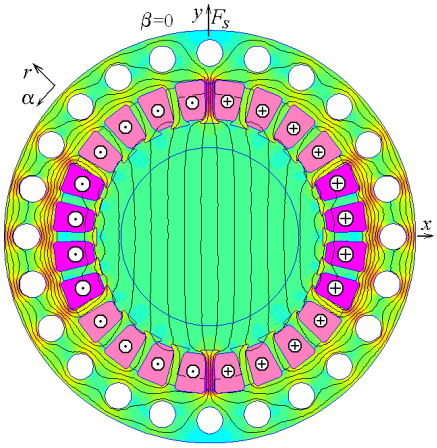

Fig. 4. Structure of the single-layer diametric winding and the magnetic field in the ideal idle mode

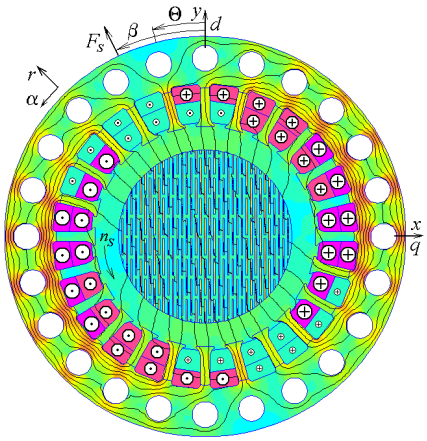

Fig. 5. Structure of the two-layer shortened winding and the magnetic field in rated load mode

The structure shown with a uniform distribution of FEs in the working chamber is idealized, as in [1, 10, 11], and it is required for an accessible organization of calculations. The real structure of the elements is usually less ordered.

FEs are made of steel St3. Their sizes and intervals between them are taken as in [11], which can be understood in Fig. 5, where everything is depicted on a single scale. An important parameter is the fill factor of the chamber with them in the *xy*-plane K_{Fes}, which is 0.32. The same coefficient is taken in the *yz*-plane: then the volume fill factor K_{Fev} has a value of 0.1.

For the winding options considered in Fig. 4, 5, the operating modes can be changed, but in general the pictures of the magnetic field are almost preserved.

In the cross section of the IRMF (see Fig. 1), the magnetic field is considered plane-parallel [10]. Therefore round sections of FEs are replaced by square ones with the corresponding recalculations of the sizes.

Fundamentals of numerical field calculations. The source of the rotating magnetic field in the inductor is a three-phase system of currents of the phase windings:

$$\begin{aligned} i_A &= I_m \cos(\omega_s t + \beta); \\ i_B &= I_m \cos(\omega_s t - 2\pi/3 + \beta); \\ i_C &= I_m \cos(\omega_s t + 2\pi/3 + \beta), \end{aligned} \tag{1}$$

where t is the time; I_m is the current amplitude; ω_s is the angular frequency; β is the initial phase of the currents, which sets the required for a particular mode of calculation angular displacement of the direction of the MMF of the stator winding F_s directed by the *y*-axis.

An example of this is shown in Fig. 5, where β=26.7°. Figure 4 shows the directions of currents in the phase windings in the II mode, in which β=0, and therefore the vector of the MMF F_s is directed along the *y*-axis.

The magnetic field of the inductor in its central cross section is described by the well-known 2D differential equation [10, 12]:

$$\mathrm{rot}[\mu_a^{-1}\mathrm{rot}(\vec{k}A_z)] = \vec{k}J_z, \tag{2}$$

where μ_a is the absolute magnetic permeability; $\vec{k}$ is the unit vector along the axial *z*-axis; A_z, J_z are the components of the magnetic vector potential and current density.

The propagation of the magnetic field is limited by the Dirichlet boundary condition A_z = 0 on the outer surface of the core. The effect of the camera shell on the magnetic field is considered insignificant.

The provided research tools are numerical calculations of the magnetic field by the Finite Element Method according to the FEMM computer code [12] with control by the created Lua script. In general, the method of calculating the magnetic fields of the inductor and its electromagnetic parameters, as well as the rationale for the accepted assumptions are described in detail in [10, 11], so in this work this is not repeated.

The voltage equilibrium in the phase winding of the stator corresponds to the complex equation [10]:

$$\underline{U}_s = -\underline{E}_a + jX_v\underline{I}_s + (R_s + R_{mag})\underline{I}_s, \tag{3}$$

where the complexes of its current $\underline{I}_s$ and EMF $\underline{E}_a$, which is created on the active length of the winding, are presented.

Formula (3) also includes the active resistance R_s and the reactive resistance of the frontal scattering X_v of the phase winding, as well as the active resistance R_{mag}, which reflects the power of the magnetic losses and is determined during the iterative calculation of the magnetic field [10].

Comparative calculations of geometric parameters of winding variants in the inductor. Figures 4, 5 already show the accepted shape of the semi-closed slot of the inductor, which is trapezoidal with rounding, which is characteristic of induction motors of the same size.

Figure 6 shows the structure of the insulation of the slot, which for the two-layer winding is supplemented by a jumper. Detailed calculations show that in the case of a single-layer winding, the useful cross-sectional area of the slot remaining for the conductors, S_{sn}=274 mm^2, and in the case of a two-layer winding, it decreased by 4 mm^2 or 1.5 %.

For clarity of further illustrations for the winding, the adopted diameter of the uninsulated effective conductor d_{sc} = 3 mm, and of the insulated one is d_{scis} = 3.46 mm, and in the slot their number is z_{Qs} = 18. For technological reasons, the effective conductor can be divided into elementary conductors of smaller diameter.

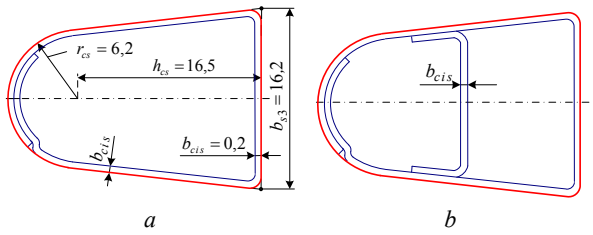

Fig. 6. Estimated model of the slot with insulation (b_{cis} – insulation thickness): *a* – with a single-layer winding, *b* – with a two-layer winding (dimensions in mm)

The main difference between the given variants of a winding consists in their frontal parts, and here the careful calculation analysis is applied.

The design of the frontal parts of the single-layer concentric winding is shown in Fig. 7 – in the longitudinal section of the inductor, as well as in Fig. 8 as a view of the ends of these parts.

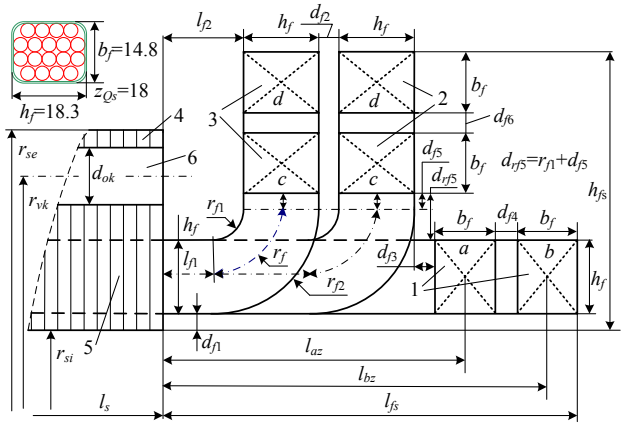

Fig. 7. Frontal part of the concentric winding in the meridian section: 1, 2, 3 – phase windings; 4 – surface of the core; 5 – slot with the winding rod; 6 – axial ventilation channel

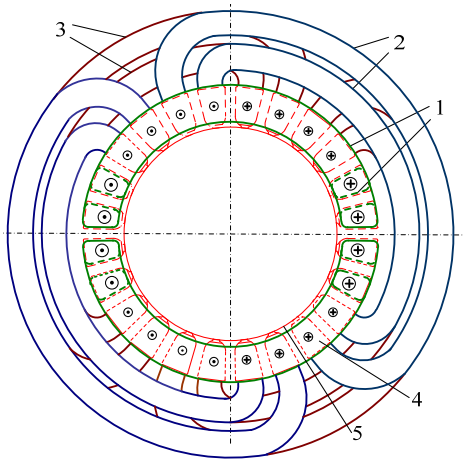

Fig. 8. Frontal part of the concentric winding (end view): 1, 2, 3 – phase windings; 4 – slot with the winding rod; 5 – core boring surface

The whole structure depends on the size of the «harness» of the conductors, which is formed in a rectangular section, and Fig. 7 shows its dimensions h_f and b_f (in mm) together with the surface insulation. The figure is shown in proportion, and all dimensions are marked on it without providing a number of values just to reveal the degree of detail of the calculations.

The design of the frontal parts of the two-layer loop winding is given in Fig. 9, where two sections are left from a flat scan (see Fig. 3), as well as a view in longitudinal section of the inductor (right). Here, one harness contains half the number z_{Qs}, i.e. 9 conductors, and its dimensions h_f and b_f together with the insulation were 11 mm. In Fig. 9, as in Fig. 7 the proportions of the sizes are saved, but all set of their designations is shown for display of a measure of detailing of calculations.

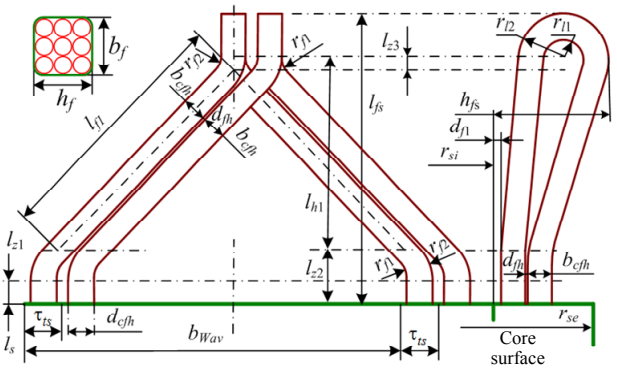

Fig. 9. Calculation model of the frontal part of the loop two-layer winding with indication of the size of its elements

The frontal parts of the windings are sparse, gaps are provided between them. This is necessary in conditions of high current density in the winding and a complicated cooling and ventilation system in the inductor compared to induction motors. Facilitation of cooling and ventilation is achieved by the introduction of axial ventilation ducts in the stator core, which is not practiced in induction motors of appropriate dimensions. However, the study of this issue is beyond the scope of this article and will be considered separately.

On the basis of calculation models of frontal parts of windings, detailed calculations of their sizes are carried out that allows to carry out their comparative analysis. First of all, Table 1 shows the basic geometrical parameters of two variants of the inductor winding (hereinafter 1*sl* – single-layer concentric diametrical; 2*sl* – two-layer shortened loop).

Table 1

Lengths of the elements of single- and double-layer windings

Version	h_{fs}	l_{fs}	l_{fhav}	l_{Wav}	l_{csav}
	mm	mm	mm	mm	m
1*sl*	70	103	460	1420	102
2*sl*	58	145	379	1259	91

The dimensions indicated in Table 1: h_{fs} – the farthest deviation of the winding from the boring core; l_{fs} – the outreach of the frontal part of the winding; l_{fhav} and l_{Wav} – the length of the wire of the frontal part and the coil of the average coil; l_{csav} – the length of the wire of the average phase winding.

The average length of the coil is the sum of the lengths of the rectilinear slot l_s and the curved frontal parts l_{fhaw} of the winding:

$$l_{Wav} = 2(l_s + l_{fhav}). \quad (4)$$

The total length of the conductors of the phase winding

$$l_{cs} = l_{Wav} N_s. \quad (5)$$

According to the indicators h_{fs} and l_{fs} (Fig. 7, 9), which affect the dimensions of the inductor, the windings have both advantages and disadvantages, but in terms of the volume $h_{fs}\times l_{fs}$ the double-layer winding loses by 17 %, although in the total volume of the inductor it will have a much smaller share. But the gain in diameter through h_{fs} has priority over the loss in axial length through l_{fs}.

The structure of the sections of the loop winding (see Fig. 3) is always symmetrical. The concentric winding has six different variants of the coils (Fig. 2), and their asymmetry (see Fig. 7) occurs due to different lengths of the wire of the frontal parts l_{favh}. But for comparison in Table 1 the lengths l_{fhav} and l_{Wav} of the average coil are taken. As a result, the loop winding has the advantage of a shorter wire length l_{cs} of the phase winding by 12 %. In addition to saving copper, this helps to reduce the active and reactive resistance of this winding.

However, the disadvantages of the concentric winding are manifested not only in this, but also in the asymmetry of the phase windings as a whole due to the difference of their individual coils, which is explained in Table 2. Here the calculated dimensions of the elements of this winding are indicated: l_{fhawk}, l_{Wavk} – the average lengths of the frontal parts and individual coils; l_{Wavf}, l_{csf} – the average lengths of turns and all wire of phase windings, and the made designations of versions of coils correspond to Fig. 7: 1, 2, 3 – the number of phase winding; *a*, *b*, *c*, *d* – the version of its coil.

Table 2

Lengths of the elements of the concentric winding

Version	1*a*	1*b*	2*c*	2*d*	3*c*	3*d*
l_{fhawk}, mm	324	402	429	635	382	589
l_{Wavk}, mm	1149	1305	1357	1770	1264	1677
l_{Wavf}, m	1227		1564		1471	
l_{csf}, m	88		113		106	

Manifestation of asymmetry is the difference of the largest and smallest sizes: l_{fhawk} by 96 %, l_{Wavk} by 54 %, l_{Wavf} and l_{csf} by 28 %, and the reason for this is the frontal parts of the phase windings.

For low and medium power machines for practical calculations empirical formulas that take into account the main features of the design forms of the coils are used [9]. For the coil of the bulk concentric winding of the stator, the following winding lengths are obtained: l_{cs} = 80.3 m; l_{Wav} = 1115 mm; l_{fh} = 307 mm; l_{fs} = 75.2 mm. It is seen that the classical technique, in comparison with the developed method, gives significantly underestimated parameters of the windings l_{cs} and l_{Wav} – by 21 %; l_{fh} – by 33 %; l_{fs} – by 27 %. That is, the classical approximate technique does not take into account the features of the stator winding of this inductor.

For a two-layer loop shortened winding the classical technique according to the corresponding formulas gives lengths: l_{fh} = 302 mm, l_{fs} = 97.5 mm, l_{Wav} = 1104 mm, l_{cs} = 79.5 m, which differs from the developed refined method by 20.3 %, 32.8 %, 12.6 % and 12.3 %, respectively.

Stator phase winding resistances. The calculated geometric parameters of the windings allow to determine their active resistances and reactive resistances of the frontal scattering included in (3). Reactive scattering resistances on the active length of the winding are automatically taken into account in the EMF E_a, which is determined by calculating the magnetic field at this length.

Active electrical resistance of the phase winding, reduced to the accepted operating temperature T_w = 115 °C:

$$R_s = k_r\, k_{T\,Cu}\, \frac{\rho_{Cu\,Tb}\; l_{cs}}{S_{s\,c}}, \qquad (6)$$

where S_{cs} is the cross section of the effective conductor, m^2; ρ_{Tb} = 1.75 10^{-8} Ω·m is the resistivity of copper winding at base temperature T_b = 20 °C; $k_{TbCu} = 1+\alpha_T\cdot(T_w - T_b)$ is the temperature coefficient of resistance (k_{TbCu}=1,38); α_T = 0.004 °C^{-1} is the specific temperature coefficient of resistance of copper; k_r is the coefficient of increase of resistance due to current displacement (following [9], k_r = 1).

Inductive resistance of the frontal scattering of the phase winding of the stator is determined by the classical method [9], which is common to given types of winding:

$$X_v = 1{,}58\cdot\frac{f_s\, l_s\, N_s^2\, \lambda_{\sigma\, fh}}{p\; q_s\, 10^8}, \qquad (7)$$

where the scattering conductivity factor of the frontal parts of the stator winding

$$\lambda_{s\,fh} = 0{,}34\frac{q_s}{l_s}\left(l_{fh} - 0{,}64\beta_s\,\tau_p\right); \qquad (8)$$

where q_s is the number of slots per pole and phase.

Comparison of resistances (p.u.) of single-layer (1*sl*) and double-layer (2*sl*) windings are given in Table 3. The advantage of the second of them in terms of resistance is obvious: active resistance is 11 % lower, reactive resistance of frontal scattering is lower by 18 %. When calculating for a concentric winding, its parameters are taken as average, accordingly, the parameters in Table 3 are averaged.

Table 3

Electrical parameters of windings

Version	R_s	$\lambda_{s\,fh}$	X_v	I_s	E_a	U_v	U_R
	Ω	p.u.	Ω	A	V	V	V
1*sl*	0,349	1,847	0,473	59,9	69,4	28,3	21,6
2*sl*	0,310	1,516	0,378	66,5	72,0	25,1	21,4

The conditional active resistance R_{mag} included in (3) depends on the load level of the inductor and is in the range 0.01–0.014 Ω.

Analysis of the electromagnetic parameters of the inductor in the ideal idle mode. The initial calculations of the electromagnetic parameters of the inductor are performed in the II mode, the essence of which is the absence of ferromagnetic elements in the working chamber. It is for this mode that the required value of the magnetic flux density B_{av} in this chamber is set, and it is the most intense in terms of the stator winding current that given in [11].

At rated voltage U_{sN}, the effective values of current I_s, EMF E_a and voltage drops $U_v = X_v I_s$ and $U_R = (R_s+R_{mag})I_s$ have the values shown in Table 3. There is a significant effect on the equilibrium of voltages of their drops, which leave for the main EMF about 70 % of

the input voltage, while, for example, in induction motors it reaches more than 95 %.

Electrical and energy parameters of the inductor for the two versions of the winding in the II mode are given in Table 4, where P_{els}, P_{mags} – the power of electric and magnetic losses; J_{sc} – the current density in the conductor; A_s – the linear current load on the core boring.

Table 4

Comparison of electrical and energy inductor parameters when using different windings

Version	P_{els}	P_{mags}	B_{av}	J_{sc}	A_s
	W	W	T	A/mm^2	A/cm
1*sl*	3760	43	0,117	8,48	687
2*sl*	4100	41	0,125	9,40	761

Graphs of distribution of the module of the magnetic flux density B in the core of the inductor are given in Fig. 10, 11. They correspond to the II for a symmetric current system with the values in Table 3 (for a concentric winding it is conditional with averaging of phase windings).

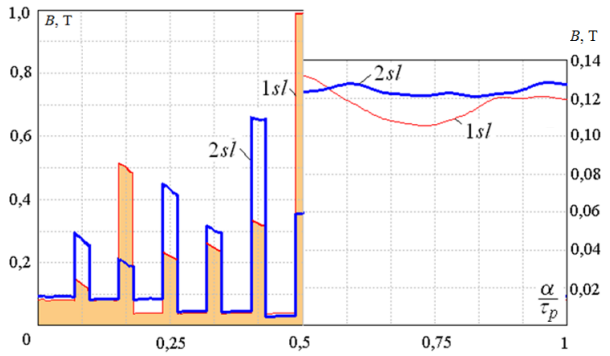

Fig. 10. Distribution of the magnetic flux density along the pole arc (left – on the average radius along the height of the tooth, right – on the surface of the working chamber)

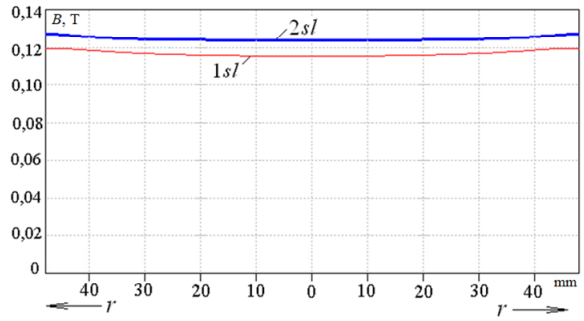

Fig. 11. Distribution of the magnetic flux density along the horizontal central axis within the working chamber

The graphs show that from the point of view of uniformity of distribution of the magnetic flux density the loop shortened winding has an advantage, besides it gives slightly more value of the magnetic flux density in the working chamber. And the nonuniform distribution in both cases is caused by the discrete structure of the stator winding.

If we consider the individual phase windings, then in its loop version, symmetry is its essence. Consequently, in the case of a concentric winding, due to differences in the parameters of the phase windings (see Table 2), there is a significant asymmetry of the phase currents and other electrical quantities. And this leads to known problems, the basis of the analysis of which is the following approximate method.

The reactive resistance of the slot part of the winding $X_a = E_a/I_s$ is introduced, which was 1.159 Ω and essentially takes into account the mutual inductive resistances of all phases, because the phase EMF E_a was determined by the magnetic field of the entire three-phase winding.

The difference in the parameters of the three windings arose due to the different lengths of their frontal parts, given in Table. 5. Therefore, there are active R_s and reactive X_v resistance, which are shown in the same table.

Table 5

Comparison of inductor phase parameters for concentric winding

Phase winding	l_{fh}	X_v	R_s	Z_s	I_s
	mm	Ω	Ω	Ω	A
1	363	0,473	0,275	1,529	65,30
2	532	0,573	0,403	1,776	56,16
3	486	0,508	0,368	1,708	58,55
av	460	0,473	0,349	1,671	59,85

To eliminate the «skew» of the phase voltages, the concentric winding is fed by a «star» circuit with a neutral wire N (Fig. 2). Then the separate impedance for each phase

$$Z_s = \sqrt{(R_s + R_{mag})^2 + (X_a + X_v)^2} \qquad (9)$$

and the phase current $I_s = U_s/Z_s$ are calculated.

The obtained asymmetric current system is given in Table 5. In addition to the parameters of the numbered phase windings 1, 2, 3, it also presents the parameters of the averaged winding *av*.

The obtained effective values of phase currents are substituted in (1), and a number of calculations of the magnetic field when changing β from 0 to 180° with a step of 2° is carried out, which provided a simulation of the rotation of the magnetic field.

At each calculation point, the values of the magnetic flux density were determined at fixed points of the working chamber: 1 – in the center; 2, 3 – in the upper and right boundary points.

The results of calculations for the asymmetric concentric winding are given in Fig. 12 compared to similar graphs for a symmetrical loop winding. The graphs show the advantage of a loop winding, which provides almost stable magnetic flux density. With a concentric winding, there are significant pulsations of the magnetic flux density, because the asymmetric current system gives an elliptical magnetic field.

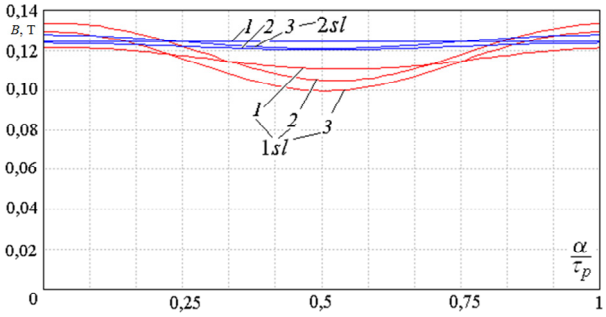

Fig. 12. Changes in the magnetic flux density at fixed points of the working chamber during the rotation of the magnetic field: 1 – in the center; 2, 3 – on the surface at the top and right

Conclusions.

1. The developed technique allows on the basis of a single approach to calculate the geometric parameters of the frontal parts of concentric and loop windings taking into account their detailed structure and size of all components, which gives much more accurate results compared to classical methods of designing electric machines.

2. In the conditions of the inductor of a magnetic field the role of frontal parts of windings appears much more essential, than in the conditions of classical AC machines. This is manifested in an increase of 5-6 times the relative contribution to the equation of equilibrium of the EMF and the voltage drops on the reactance of the frontal scattering, as well as on the active resistance of the windings.

3. An important advantage of the loop shortened winding compared to the concentric diametric winding is the shorter length of the frontal part conductor, which reduces the active resistance of the winding as a whole by 11 % and the reactance of the frontal scattering by 18 %.

4. The loop three-phase winding is symmetrical, while the concentric winding has a pronounced asymmetry due to differences in the parameters of its frontal parts, which leads to a significant deterioration of the electromagnetic parameters of the inductor as a whole.

5. Due to the peculiarities of the discrete phase structure of the concentric diametric winding and the asymmetry of its phase currents, the magnetic field in the working chamber of the inductor is unstable and less homogeneous compared to the loop shortened winding.

6. The advantages of the concentric winding include a slightly smaller particle size of the inductor in the area of its frontal parts, as well as less complex technology of manufacturing and laying in the slots of the core.

7. Further development of research should be the development of technology for the manufacture of loop shortened two-layer winding in the inductor conditions, the implementation of its relevant experimental studies, as well as improving the parameters of this winding by optimizing it.

Conflict of interest. The authors declare that they have no conflicts of interest.

REFERENCES

1. Logvinenko D.D., Sheljakov O.P. *Intensifikacija tehnologicheskih processov v apparatah s vihrevym sloem* [Intensification of technological processes in apparatus with a vortex layer]. Kiev, Tehnika Publ., 1976. 144 p. (Rus).

2. Belounis A., Mehasni R., Ouil M., Feliachi M., El-Hadi Latreche M. Design with optimization of a magnetic separator for turbulent flowing liquid purifying applications. *IEEE Transactions on Magnetics*, 2015, vol. 51, no. 8, pp. 1-8. doi: https://doi.org/10.1109/tmag.2015.2424401.

3. *Company GlobeCore. Vortex Layer Machine ABC-100.* Available at: https://avs.globecore.ru/products/avs-100.html (accessed 30 September 2017). (Rus).

4. Ogonowski S., Wołosiewicz-Głąb M., Ogonowski Z., Foszcz D., Pawełczyk M. Comparison of wet and dry grinding in electromagnetic mill. *Minerals*, 2018, vol. 8, no. 4, p. 138. doi: https://doi.org/10.3390/min8040138.

5. Wolosiewicz-Glab M., Ogonowski S., Foszcz D., Gawenda T. Assessment of classification with variable air flow for inertial classifier in dry grinding circuit with electromagnetic mill using partition curves. *Physicochemical Problems of Mineral Processing*, 2018, vol. 54, no. 2, pp. 440-447. doi: http://dx.doi.org/10.5277/ppmp1867.

6. Całus D., Makarchuk O. Analysis of interaction of forces of working elements in electromagnetic mill. *Przegląd Elektrotechniczny*, 2019, no. 12, pp. 64-69. doi: https://doi.org/10.15199/48.2019.12.12.

7. Shvedchykova I., Melkonova I., Romanchenko J. Research of magnetic field distribution in the working area of disk separator, taking into account an influence of materials of permanent magnets. *EUREKA: Physics and Engineering*, 2020, vol. 1, pp. 87-95. doi: https://doi.org/10.21303/2461-4262.2020.001106.

8. Makarchuk O., Calus D., Moroz V. Mathematical model to calculate the trajectories of electromagnetic mill operating elements. *Technical Electrodynamics*, 2021, no. 2, pp. 26-34. doi: https://doi.org/10.15407/techned2021.02.026.

9. Kopylov I.P., Klokov B.K., Morozkin V.P., Tokarev B.F. *Proektirovanie elektricheskih mashin* [The design of electrical machines]. Moscow, Yurait Publ., 2011. 767 p. (Rus). Available at: https://em.fea.kpi.ua/images/doc_stud/distsiplini/oapem2/kopilov_proektirovanie_em_2011.pdf (accessed 10 May 2021).

10. Milykh V.I., Shilkova L.V. Characteristics of a cylindrical inductor of a rotating magnetic field for technological purposes when it is powered from the mains at a given voltage. *Electrical Engineering & Electromechanics*, 2020, no. 2, pp. 13-19. doi: https://doi.org/10.20998/2074-272x.2020.2.02.

11. Milykh V.I., Shilkova L.V. Control current method of the concentration of ferromagnetic elements in the working chamber of the technological inductor of magnetic field during its operation. *Electrical Engineering & Electromechanics*, 2020, no. 5, pp. 12-17. doi: https://doi.org/10.20998/2074-272x.2020.5.02.

12. *Finite Element Method Magnetics: OldVersions.* FEMM 4.2 11Oct2010 Self-Installing Executable. Available at: http://www.femm.info/wiki/OldVersions (accessed 15 May 2021).

Received 15.05.2021
Accepted 20.06.2021
Published 27.08.2021

V.I. Milykh[1], *Doctor of Technical Science, Professor,*
M.G. Tymin[1], *Postgraduate Student,*
[1] National Technical University «Kharkiv Polytechnic Institute», 2, Kyrpychova Str., Kharkiv, 61002, Ukraine,
e-mail: mvikemkpi@gmail.com (Corresponding author),
gunter_odim@ukr.net

How to cite this article:
Milykh V.I., Tymin M.G. A comparative analysis of the parameters of a rotating magnetic field inductor when using concentric and loop windings. *Electrical Engineering & Electromechanics*, 2021, no. 4, pp. 12-18. doi: https://doi.org/10.20998/2074-272X.2021.4.02.